Bioactive Materials 46 (2025) 448–456

Contents lists available at ScienceDirect

Bioactive Materials

journal homepage: www.keaipublishing.com/en/journals/bioactive-materials

Mechanically regulated microcarriers with stem cell loading for skin photoaging therapy

Xiang Lin [a,b,c,d], Anne M. Filppula [c], Yuanjin Zhao [a,d,*], Luoran Shang [e,**], Hongbo Zhang [a,b,c,f,***]

[a] Department of Gastrointestinal Surgery, The First Affiliated Hospital, Wenzhou Medical University, Wenzhou, 325035, China
[b] Joint Centre of Translational Medicine, Wenzhou Key Laboratory of Interdiscipline and Translational Medicine, the First Affiliated Hospital of Wenzhou Medical University, Wenzhou, China
[c] Pharmaceutical Sciences Laboratory, Åbo Akademi University, Turku, 20520, Finland
[d] Department of Rheumatology and Immunology, Nanjing Drum Tower Hospital, School of Biological Science and Medical Engineering, Southeast University, Nanjing, 210096, China
[e] Shanghai Xuhui Central Hospital, Zhongshan-Xuhui Hospital, and the Shanghai Key Laboratory of Medical Epigenetics, International Co-laboratory of Medical Epigenetics and Metabolism (Ministry of Science and Technology, Institutes of Biomedical Sciences), Fudan University, Shanghai, 200032, China
[f] Turku Bioscience Centre, University of Turku and Åbo Akademi University, Turku, 20520, Finland

ARTICLE INFO

Keywords:
Microcarriers
Mechanical regulation
Hydrogel
Stem cell
Photoaging therapy

ABSTRACT

Long-term exposure to ultraviolet radiation compromises skin structural integrity and results in disruption of normal physiological functions. Stem cells have gained attention in anti-photoaging, while controlling the tissue mechanical microenvironment of cell delivery sites is crucial for regulating cell fate and achieving optimal therapeutic performances. Here, we introduce a mechanically regulated human recombinant collagen (RHC) microcarrier generated through microfluidics, which is capable of modulating stem cell differentiation to treat photoaged skin. By controlling the cross-linking parameters, the mechanical properties of microcarriers could precisely tuned to optimize the stem cell differentiation. The microcarriers are surface functionalized with fibronectin (Fn)-platelet derived growth factor-BB (PDGF-BB) to facilitate adipose derived mesenchymal stem cells (Ad-MSCs) loading. In *in vivo* experiments, subcutaneous injection of stem cell loaded RHC microcarriers significantly reduced skin wrinkles after ultraviolet-injury, effectively promoted collagen synthesis, and increased vascular density. These encouraging results indicate that the present mechanically regulated microcarriers have great potential to deliver stem cells and regulate their differentiation for anti-photoaging treatments.

1. Introduction

Skin aging is an inherent physiological phenomenon, characterized by increased fragility, lower tissue integrity, and a decline in repair ability [1–4]. External factors, especially ultraviolet radiation, can further accelerate skin aging [5–9]. Traditional anti-aging methods, such as the use of cosmetological care products, medicines, or dermal fillers, are developed to improve skin elasticity and reduce wrinkles [10–16]. However, these methods involve foreign substances that may carry risks of toxicity and tend to offer only temporary anti-aging benefits [17,18]. Recent strides in stem cell therapy have shown promise for revitalizing aged skin through anti-inflammatory and antioxidant factors [19–22]. However, these therapies currently face significant challenges. For example, intravenously injected stem cells often show low survival rates, and their unpredictable differentiation in the body can lead to inconsistent treatment results [23,24]. In addition, temporary application via a single dose injection cannot achieve long-term anti-aging effects [25,26]. Therefore, there is a critical demand for enhancing the survival, integrity, and functional longevity of stem cells in skin rejuvenation treatments.

In this study, we introduce a mechanically regulated human recombinant collagen microcarrier fabricated with microfluidics, which

* Corresponding author. Department of Gastrointestinal Surgery, The First Affiliated Hospital, Wenzhou Medical University, Wenzhou, 325035, China.
** Corresponding author.
*** Corresponding author. Department of Gastrointestinal Surgery, The First Affiliated Hospital, Wenzhou Medical University, Wenzhou 325035, China.
E-mail addresses: yjzhao@seu.edu.cn (Y. Zhao), luoranshang@fudan.edu.cn (L. Shang), hongbo.zhang@abo.fi (H. Zhang).

https://doi.org/10.1016/j.bioactmat.2024.12.024
Received 22 August 2024; Received in revised form 25 November 2024; Accepted 21 December 2024
Available online 3 January 2025

can modulate stem cell differentiation and treat photoaged skin (Fig. 1). Microfluidic technology can be used for the fabrication of various types of microcarriers [27–31]. In particular, the microcarriers constructed from protein components, such as human recombinant collagen, are also suitable for cell culture [32–35]. However, existing microcarriers still face the tradeoff between tunable mechanical properties and structural stability, making it difficult for regulating differentiation in adipose-derived mesenchymal stem cells (Ad-MSCs) [36]. The elastic modulus of extracellular matrix is a crucial mechanical cue for training stem cells. Numerous *in vitro* studies have demonstrated that substrates replicating the stiffness of specific tissues can effectively direct stem cells toward differentiation into corresponding tissue types [37,38]. Therefore, it can be conceived that tunable mechanical properties are essential for microcarriers to provide appropriate mechanical microenvironments for delivered stem cells, thus enabling effective stem cell-based anti--photoaging therapies.

To realize this, droplet microfluidic technology was employed to fabricate recombinant human protein microcarriers with uniform size. By adjusting the substitution degree of methacrylic anhydride as well as ultraviolet exposure duration, the mechanical properties of microfluidic generated RHC microcarriers were precisely modulated. In addition, the "Ultrasoft" RHC microcarriers were coated with fibronectin (Fn) and further integrated with the exogenous factor platelet-derived growth factor-BB (PDGF-BB), which provided a favorable substrate for cell growth. Ad-MSCs were successfully loaded onto the microcarriers. Moreover, the Ad-MSC loaded RHC microcarriers showed their ability to resist the apoptosis and Reactive Oxygen Species (ROS) generation of photoaging Human Immortalized Epidermal Cells (HaCaT) cells *in vitro*. The animal experiments revealed that the present Ad-MSC microcarriers significantly mitigated UV-induced skin wrinkles, stimulated collagen production, and increased vascular density. We believe that the mechanically regulated stem cell microcarriers can pioneer a novel approach in anti-photoaging therapies.

1.1. Experimental section

In a typical experiment, type III collagen was obtained from genetically engineered yeast expressing the RHC protein gene, as illustrated in Fig. 2a. This collagen has a triple helical structure and exhibits excellent cell adhesion ability and biological activity. Then, we explored the generation of RHC hydrogels with tunable mechanical properties through chemical crosslinking under varying parameters. Briefly, methacrylated RHC (RHCMA) was synthesized by reaction with methacrylic anhydride (MA) following previously reported protocols. The RHCMA exhibited new peaks of methacryloylated grafts and was able to form a stable hydrogel after ultraviolet irradiation (Fig. 2b–c). Afterwards, we studied the correlation between the mechanical properties of photo-crosslinked RHCMA hydrogel and the experimental parameters. We found that RHCMA hydrogels with different mechanical properties can be obtained by tuning the degree of MA substitution (Fig. 2d) and curing time (Fig. S1 and Table S1). With that, we named four types of RHCMA hydrogels based on their modulus, including Ultrasoft (1.3 kPa), Soft 6.7 (kPa), Stiff (9.3 kPa), and Ultrastiff (21.4 kPa). Furthermore, we seeded Ad-MSCs onto hydrogels with different modulus to test the adipogenic differentiation. After seven days of induction with adipogenic differentiation induction medium, the Oil Red O staining results indicated that softer RHC hydrogels tended to promote the adipogenic differentiation of Ad-MSCs more effectively (Fig. 2e–f).

A microfluidic device used for microcarrier generation was prepared with two capillary tubes of the same outer diameter (Fig. S2a). The inner tube was drawn using a pipette puller, and the end of the tube was polished to a specific diameter using sandpaper. The tubes were integrated onto a glass slide and were coaxially aligned with the help of a square glass tube and adhesives. By injecting the RHCMA solution and silicone oil as the inner and outer phase, respectively, droplets were generated at the outlet of the inner tube due to shear force and interfacial tension (Fig. 2g). The diameter of the microcarrier could be flexibly adjusted by varying the fluid flow rates (Figs. S2b–c). We used Ultrasoft group to characterize the generated microcarriers. The

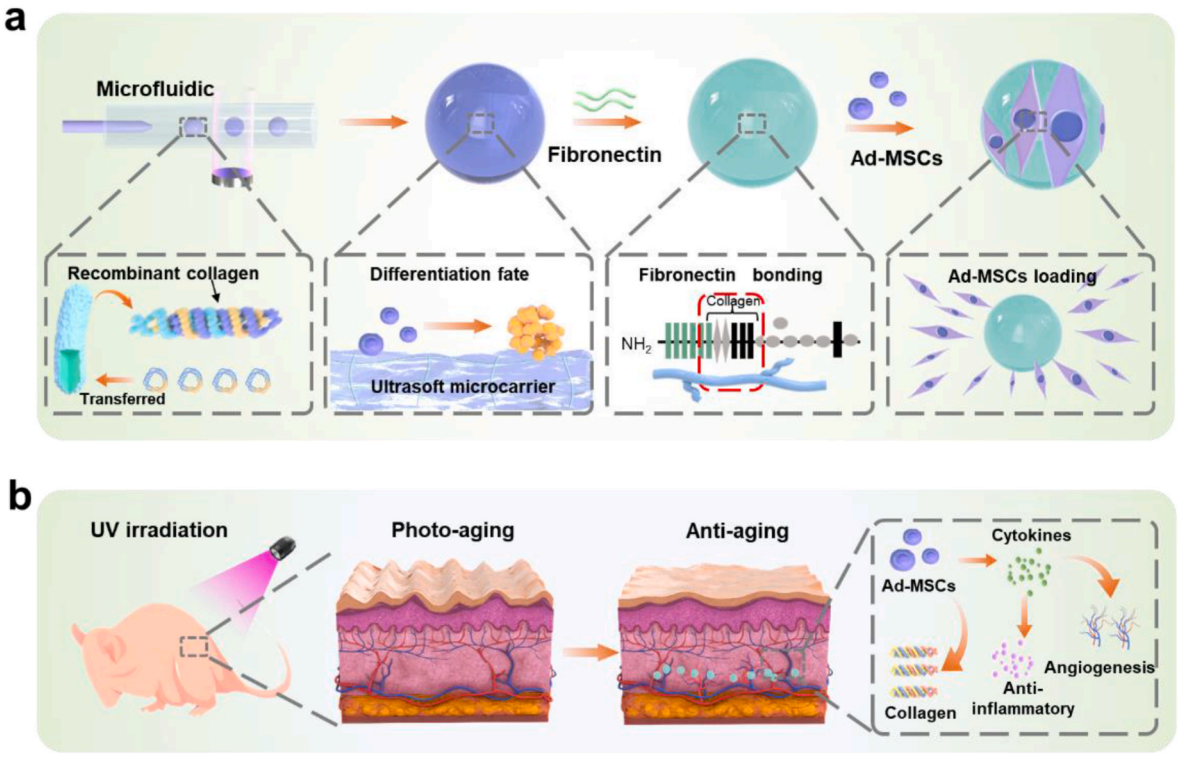

Fig. 1. Schematic illustration of a) the construction of the mechanically tunable microcarriers and the cell seeding process, and b) the treatment for photoaging mice using the stem cell loaded microcarriers.

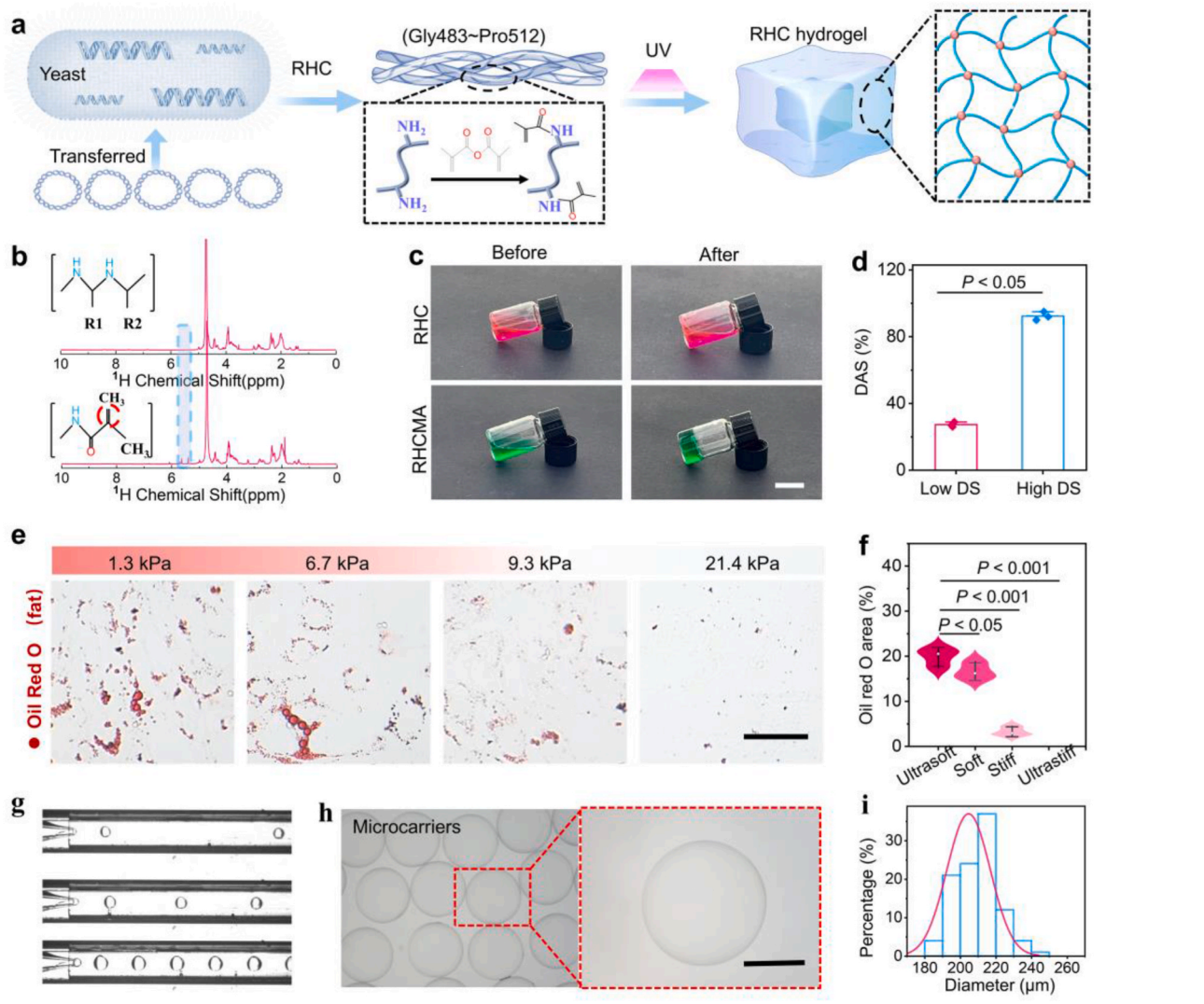

Fig. 2. a) Schematic image of the production process for RHC protein, synthesis of RHCMA, and the construction of RHCMA hydrogel via photo-polymerization. b) ^{1}H NMR results of RHC and RHCMA. c) Images of RHCMA hydrogels before and after ultraviolet irradiation. d) RHCMA with different degree of MA substitution (DAS) (n = 3). e) Oil Red O staining of mesenchymal stem cells co-cultured on hydrogels of different moduli. f) Relative oil red O area. g) The droplet generation process captured by a high-speed camera. h) Dispersed RHC microcarriers and a magnified image showing a single microcarrier. i) Particle size distribution of microcarriers (n = 100). The scale bar is 10 mm in c), 200 μm in e), 100 μm in h).

microcarriers exhibited good monodispersity and a uniform size distribution (Fig. 2h–i). These results indicated that the RHCMA was suitable for microfluidic generation of microcarriers.

To further modify the microcarrier surface with cell-recruitment factors, it is necessary to perform functionalization on the microcarriers. Since the adsorption of fibronectin (Fn) does not affect the modulus of the hydrogel, and it contains collagen/gelatin binding sites, we employed two different ligand densities of fibronectin to modify the microcarriers (Fig. 3a). Fluorescence images demonstrated strong binding of fibronectin to the RHC in the microcarriers (Fig. 3b), and the fluorescence intensity increased with an increase in fibronectin density. At two given fibronectin densities, there was no significant difference in the degree of fibronectin modification between RHC microcarriers with different moduli (Fig. 3c). The entire rheology sweep curve of hydrogels with different mechanical properties was presented in Fig. 3d, confirming that the storage modulus of the hydrogel does not change significantly after combination (Fig. 3e). Thus, based on the results of adipogenic differentiation and Fn modification, we chose Ultrasoft microcarriers for subsequent experiments.

To further enhance the cells recruitment ability of microcarriers *in situ*, we loaded platelet-derived growth factor-BB (PDGF-BB) at the microcarriers' surface, which has been demonstrated to initiate endogenous stem cell recruitment (Fig. 4a). The encapsulation efficiency of the modified microcarriers was higher compared with that of none modified microcarriers (Fig. S3a). Additionally, the modified microcarriers showed excellent sustained release capability, with less pronounced burst release compared to the unmodified microcarriers (Fig. S3b), indicating that Fn enhanced the combination of microcarriers and PDGF-BB. The release of PDGF-BB was as accompanied by the degradation of the microcarriers (Fig. S4). Moreover, the Ad-MSCs recruitment tests showed that the presence of PDGF-BB can further promote cell recruitment (Fig. 4b). To further assess the cell proliferation capabilities of the microcarriers, CCK8 assay was conducted and revealed that the number of cells on the surface of microcarriers containing PDGF-BB was significantly larger than unmodified group (Fig. S5). Additionally, to evaluate the cell enrichment capacity of the microcarriers, an *in vitro* MCF-10A cell scratch model was established using a Transwell insert. At different recording time points, microcarriers loaded with PDGF-BB significantly promoted cell migration (Fig. 4c–d and S6).

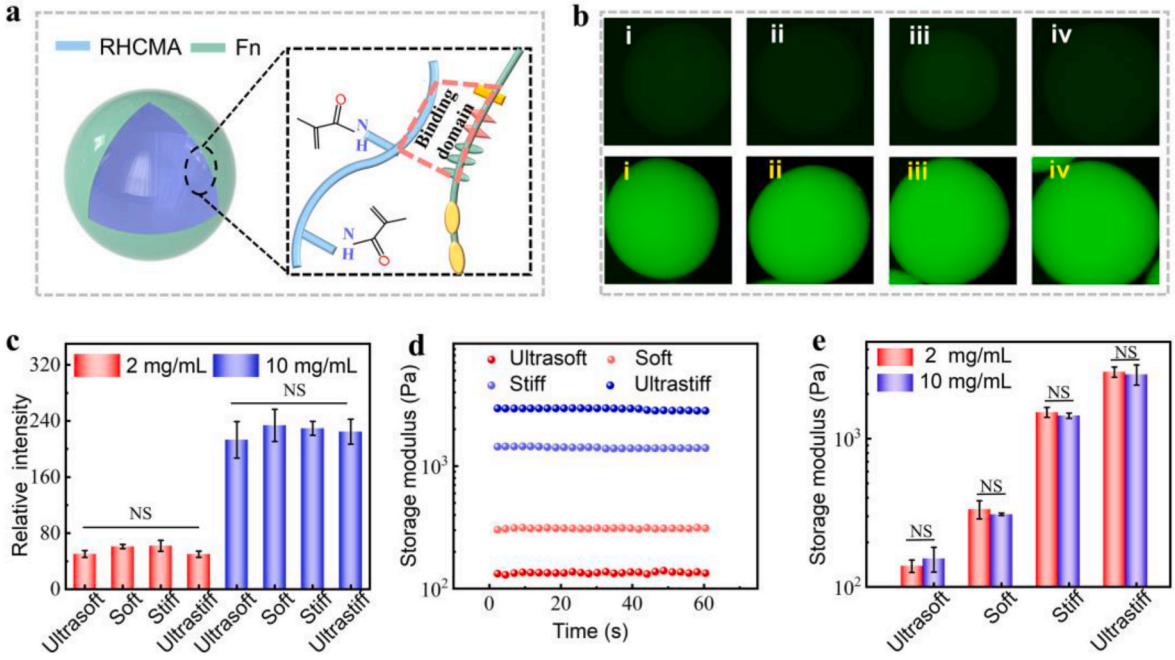

Fig. 3. a) Schematic of Fn protein grafting on the RHC microcarrier surface. b) Fluorescent images of microcarriers with different mechanical properties immersed in 2 mg/mL (white, panels i–iv) and 10 mg/mL (yellow, panels i–iv) Fn solutions for 24 h. i-iv represents the Ultrasoft, Soft, Stiff, Ultrastiff group, respectively. c) Relative fluorescence intensity in each group (n = 3). d) The time sweep curve of the storage modulus of different group hydrogels after binding with Fn protein. e) Modulus statistics for different groups of hydrogels (n = 3).

Although ultraviolet B (UVB)-induced apoptosis plays a role in maintaining skin health by removing mutated cells, prolonged UVB exposure inevitably causes adverse effects such as DNA damage, cellular aging, and can even lead to skin cell carcinogenesis. In photoaging HaCaT model, we found that the leaching medium of Ad-MSCs-loaded microcarriers (constructed by loading Ad-MSCs onto the microcarriers and co-culturing for 24 h) led to a reduction of death cell proportion (Figs. S7a–b). Additionally, following UVB irradiation, HaCaT cells produce ROS, which plays a crucial role in light-induced cell damage. We found that the intervention of Ad-MSCs-loaded microcarrier leaching media resulted in a significant decrease in ROS levels (Figs. S7c–d), suggesting that Ad-MSCs may secrete antioxidant enzymes or molecule factors,. Additionally, the aging marker SA-β-gal levels and DNA damage indicators γ-H2Ax were also significantly reduced (Figs. S7e–h). Subsequent flow cytometric analysis revealed that the experiment group treated by Ad-MSCs-loaded microcarrier leaching media exhibited a reduced proportion of apoptosis (Fig. S8). These results demonstrated that the leaching medium of Ad-MSCs-loaded microcarriers revealed a protective effect on epithelial cells against the harmful effects of UV radiation.

Ultraviolet radiation can alter specific areas of skin tissue, leading to redness, decreased skin elasticity, and the formation of wrinkles. To further investigate the anti-aging effect of the stem cell-loaded microcarriers *in vivo*, we established a photoaging nude mice model using ultraviolet irradiation and photosensitizer (8-MOP) (Fig. 5a). The skin on the back of normal mice was smooth and flawless, with few wrinkles. After UV irradiation for eight weeks, the skin became dry and peeling, and the amount of elastin in mouse skin significantly decreased (Fig. S9). The topical application of Ultrasoft RHC microcarriers (without Ad-MSCs loading) and bare Ad-MSCs alleviated skin damage caused by UV exposure. Specifically, the formation of wrinkles in the treatment group of nude mice decreased, the severity of skin surface flakes and lesions decreased, and the corresponding number of collagen fibers increased in all treatment groups (Fig. 5b–5d).

It is worth noting that the photo-aged mice treated with Ad-MSCs-loaded microcarriers showed the least number of wrinkles (Fig. 5i), which may be attributed to the fact that the stem cells loaded in the microcarriers can persist longer in the body to maintain therapeutic effects (Fig. 5f–g). The persistent survival of Ad-MSCs *in vivo* is primarily due to the biocompatibility of the microcarriers. The levels of intercellular adhesion molecule-1 (ICAM-1) were markedly decreased in the MSC and microcarrier treatment groups. This reduction could be attributed to the paracrine effects of Ad-MSCs, which helps to alleviate local inflammation. Additionally, Ad-MSCs mitigated cellular oxidative stress by suppressing the overexpression of matrix metalloproteinases, including matrix metallopeptidase 1 (MMP1) and MMP3. This inhibition subsequently enhanced the mRNA levels of collagen type I compared to the UV group (Fig. 5e and h). Moreover, improvements were also observed in dermal tissue thickness and type I collagen density in all treatment groups (Fig. 5j–k).

To further evaluate the *in vivo* therapeutic effects of the stem cell-loaded microcarriers, immunofluorescence detection was conducted. The formation of wrinkles and skin lesions in skin aging is associated with inflammation, and we found that high degrees of inflammatory factors like TNF-α, IL-6 were expressed on the UV modeling group nude mice compared to normal mice (Fig. 6a–b). MSCs release anti-inflammatory factors through paracrine signaling, thereby reducing local inflammatory responses. Mice treated with microcarriers or bare Ad-MSCs showed reduced expression of inflammatory factors, and that treated with Ad-MSCs-loaded microcarriers exhibited the lowest expression levels of inflammatory factors, suggesting the role of the microcarrier in sustaining Ad-MSCs functions (Fig. 6d–e). The photo-aged skin model group exhibited a significantly decreased dermal blood vessel density, which may be caused by the damage of the dermal extracellular matrix. Ad-MSCs can directly promote angiogenesis through the paracrine release of various pro-angiogenic growth factor like vascular endothelial growth factor (VEGF) and PDGF. Both RHC microcarrier and the topical application of Ad-MSCs group showed improved vascular numbers density (Fig. 6c and f). Importantly, the Ad-MSCs-loaded microcarrier treatment group exhibited the highest number of blood vessels, which might be attribute to the prolonged cell survival *in vivo*. These results suggest that RHC microcarriers loaded

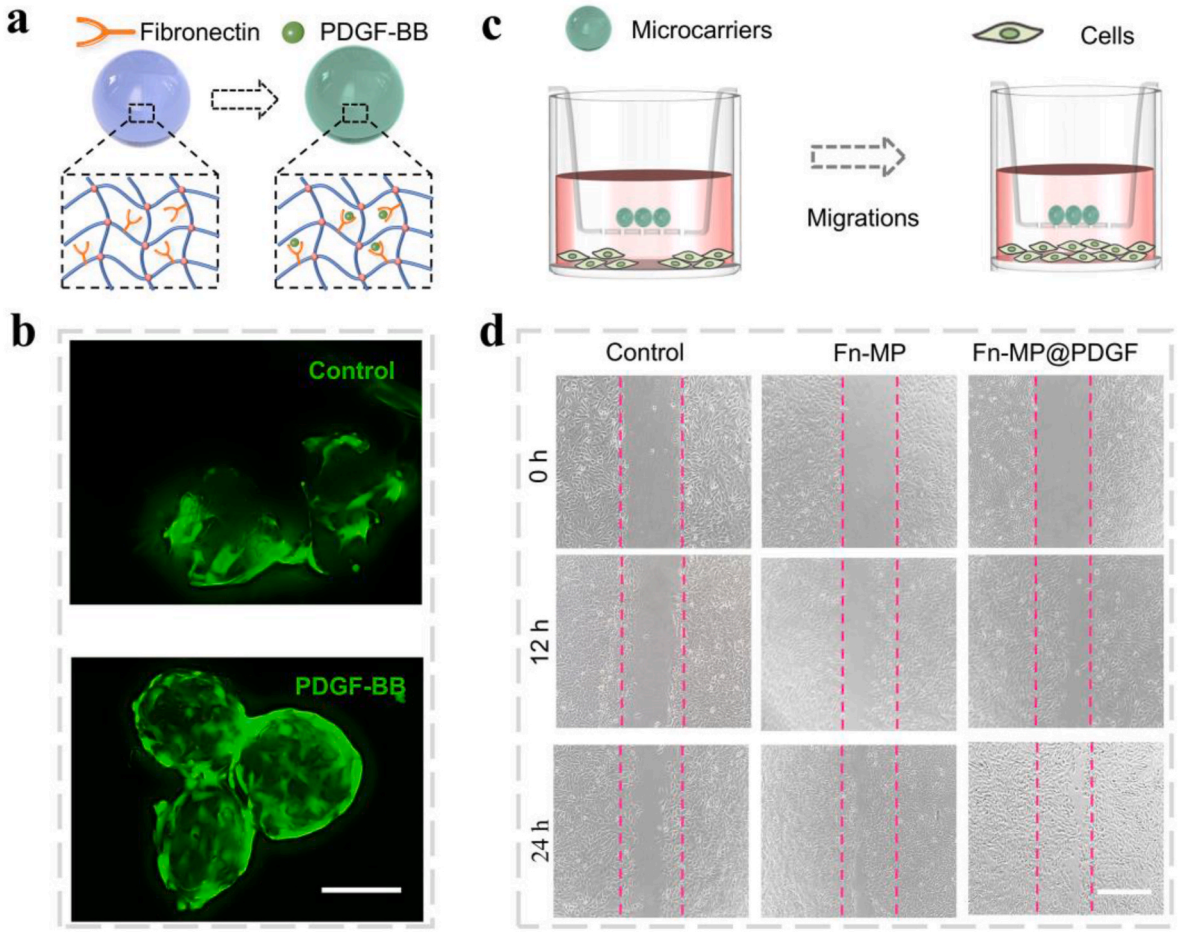

Fig. 4. a) Schematic of the process of capturing PDGF-BB factor on the surface of microcarriers with Fn protein. b) Calcein-AM staining showing live cells at the microcarrier surface: i) Control group without PDGF-BB, ii) microcarriers with PDGF-BB. c) Schematic diagram of the scratch experiment. d) Different time point images of cell migration. The scale bar is 200 μm in b) and d).

with Ad-MSCs have anti-inflammatory and pro-angiogenic effects.

Biocompatibility is a critical determinant of the therapy success, as it directly influences the host response. We further assessed the *in vivo* safety and compatibility of Ad-MSC-loaded RHC microcarriers. H&E staining revealed that RHC microcarriers loaded with Ad-MSCs did not induce obvious alterations in tissue architecture or cellular morphology in healthy mice, indicating minimal adverse effects on host tissues. Furthermore, liver function (ALT and AST) and kidney function (CREA and UA) markers were similar with those observed in the PBS control group (Fig. S10), supporting the systemic safety of the material. Fluorescence imaging via *in vivo* animal imaging demonstrated a gradual decrease in signal intensity, with only faint signals detected at day 21 (Fig. S11), indicating progressive degradation of the material. These results revealed that the Ad-MSC-loaded RHC microcarriers exhibit excellent biocompatibility positioning them as promising candidates for further clinical exploration.

2. Conclusion

In this study, we proposed a mechanically tunable RHC microcarrier via microfluidics for skin photoaging therapy. The mechanical properties of microfluidic generated RHC microcarriers was modulated by adjusting the degree of MA substitution and UV exposure time. RHC hydrogels with lower mechanical strength were found to better promote stem cell adipogenic differentiation. Additionally, Ad-MSCs were loaded on "Ultrasoft" RHC microcarriers after functionalization of Fn and PDGF-BB. *In vitro* experiments demonstrated that RHC microcarriers loaded with Ad-MSCs exhibited the ability to resist apoptosis and ROS production in photoaged HaCaT cells. In an *in vivo* photoaging model, RHC microcarriers loaded with Ad-MSCs significantly reduced UV-induced skin wrinkles, stimulated collagen production, and increased vascular density. These findings suggest that mechanically tunable microcarriers offer a novel approach in stem cell delivery as well as anti-aging therapy.

3. Methods

Materials: Recombinant human collagen (type III) was purchased from Shanxi Jinbo Bio-Pharmaceutical CO., Ltd (China), the TNBS (2,4,6-Trinitrobenzenesulfonic acid), MA were obtained from Sigma (America), fibronectin was obtained from QiYue Biotech (China) and PDGF-BB was purchased from HuaYaSiChuang Co., Ltd. (China) Primary adipose-derived mesenchymal stem cells were obtained from the Affiliated Hospital of Nanjing University. Transwell plates were purchased from Corning Inc., (America) and all PBS buffer solutions and ultrapure water used were self-prepared in the laboratory.

RHCMA generation: By varying the dosage of methacrylate anhydride (MA), different degrees of substitution of RHCMA were generated. Briefly, 10 g of RHC was dissolved in 100 mL of 0.1 M $NaHCO_3$. MA was then added dropwise to the RHC solution, with a dosage of 200 μL for low substitution RHCMA and 1 mL for high substitution RHCMA. The pH was adjusted to 9 every 10 min to promote the substitution reaction. The reaction continues for 3 h, after which the solution was filtered and further dialyzed for seven days to remove unreacted MA and other by-

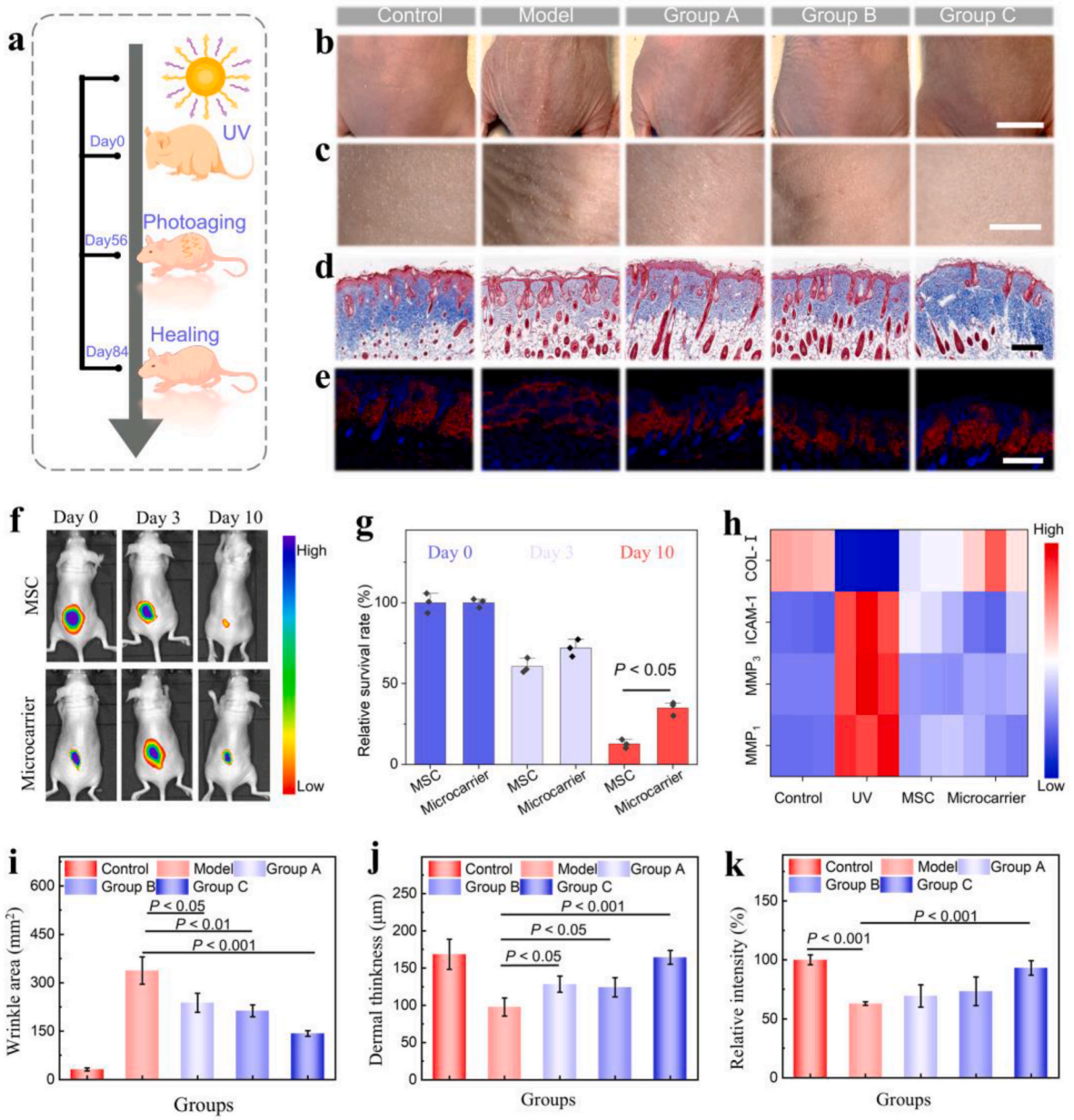

Fig. 5. a) Schematic representation of the photoaging animal experiment. b-e) The optimal images, magnified images, Masson's stained images, and immunofluorescence staining for Type I collagen of mice from different groups, Group A: RHC microcarrier group, Group B: The topical application of bare Ad-MSCs group, Group C: Ad-MSCs-loaded microcarrier group. f) *In vivo* imaging results after subcutaneous injection of DiR-labeled Ad-MSCs or DiR-labeled Ad-MSCs-loaded microcarriers in each group. g) Statistical analysis of Ad-MSCs survival rate in different time points. h) relative RT-qPCR analysis of Col-I, ICAM-1, MMP1, and MMP3 mRNA expression (n = 3). i) Statistical analysis of total wrinkle area on the back of nude mice (n = 3). j) Statistical analysis of dermal layer thickness in the skin of mice from different groups (n = 3). k) The percentage of the relative fluorescence intensity of Type I collagen density in different treatments (n = 3). The scale bar is 15 mm in b), 1 mm in Enlarged images, and 100 μm in d-e).

products.

Determination of amino substitution degree: TNBS (2,4,6-trinitrobenzenesulfonic acid) method was employed for determination of the amino substitution of RHCMA. Equal amounts (50 mg) of RHCMA as well as RHC were dissolved in 0.1 M $NaHCO_3$. The prepared 0.1 % TNBS solution was mixed with the sample solution in equal volumes (0.5 mL) and incubated for 2 h. The reaction was stopped by further adding 0.25 mL hydrochloric acid (1 M) and 0.5 mL 10 % SDS, followed by measuring absorbance at 335 nm. The amino substitution degree (D_{AS}) of RHCMA was calculated based on the changes in the number of amino groups of RHC (A_R) and RHCMA (A_{RM}):

$$D_{AS} = (A_R\text{-}A_{RM})/A_R \times 100\ \%$$

Ad-MSCs adipogenic differentiation and staining: To induce adipogenesis of Ad-MSCs on hydrogels with different mechanical strengths, Ad-MSCs were co-cultured within differentiation induction medium for three days. In brief, following instructions of the OriCell Adipogenic Differentiation Induction Kit from OriCell® (HUXMD-90031), Ad-MSCs were seeded onto the surface of the hydrogels (2×10^4 cells/cm^2). When cell density reached to 80 %, the complete culture medium was carefully removed from the wells, and adipogenic induction medium A was added (2 mL). After 72 h of induction, medium A was removed and 2 mL of medium B was added. Adipogenic differentiation was terminated after one day post-induction. For observation, 2 mL of 4 % paraformaldehyde solution were added to each well. After fixation, Oil Red O staining working solution was added into each group and stained for 30 min

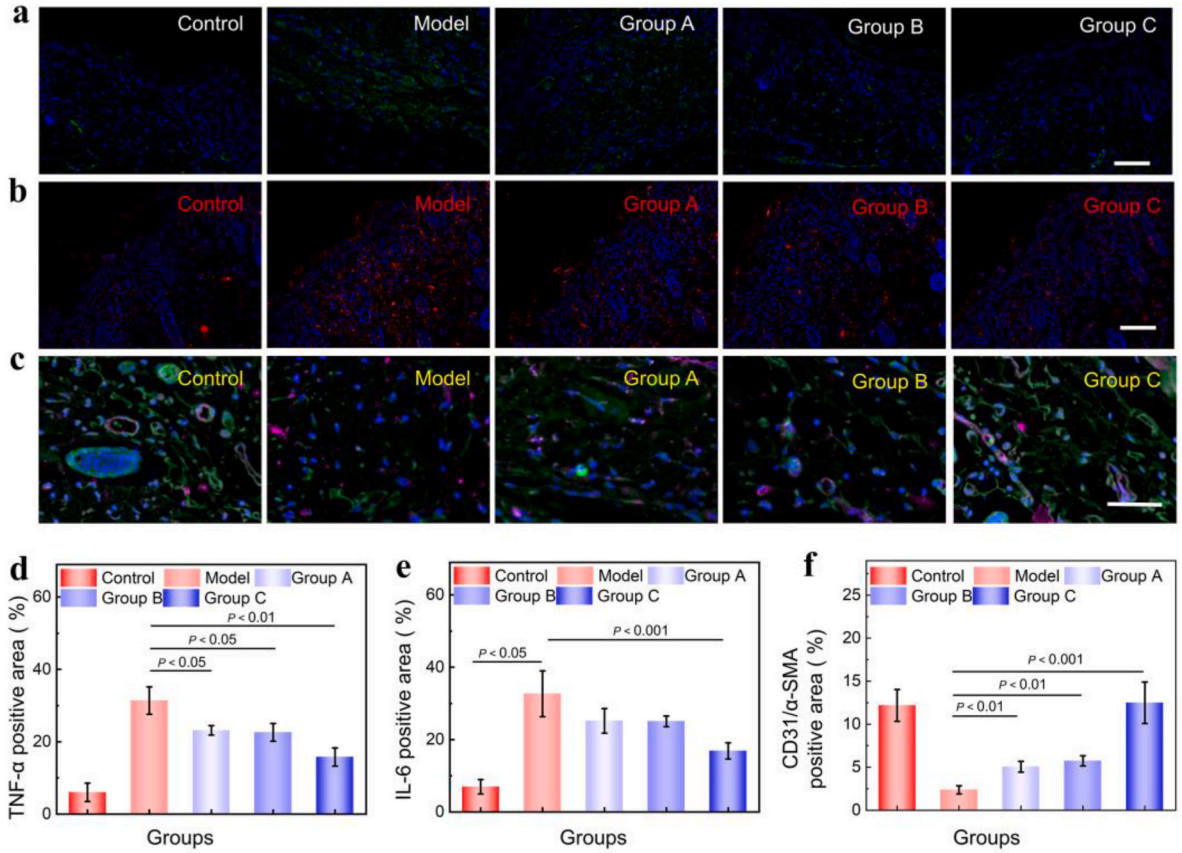

Fig. 6. a) Immunofluorescence staining showing TNF-α-positive area. b) Immunofluorescence images depicting IL-6-positive area. c) Double staining of CD31/αSMA-positive area. d) Statistical analysis of the related TNF-α-positive cells (n = 3). e) Statistical analysis of the related IL-6-positive cells (n = 3). f) Quantitative statistics of vessel density (n = 3). The scale bare is 100 μm in a-b), 50 μm in c).

(25 °C).

Microcarrier generation: A single emulsion microfluidic chip was constructed using glass capillaries. In brief, capillaries were pulled through a capillary puller, and the ends were polished to a specific diameter using a piece of sandpaper. Subsequently, one capillary was inserted into another, and the capillaries were aligned coaxially. The internal phase, pre-gel solution of RHCMA, was introduced into the injection tube, while the external phase, mineral oil, was introduced into the collection tube. Droplets were generated at the outlet of the injection tube and microcarriers were generated by further crosslinking under UV light. The microcarriers were then washed with ether and deionized water for further use.

Mechanical and rheological tests: Flattened bulk hydrogels were prepared with varying photopolymerization times and initiator concentrations (Table S1) and were subjected to compression testing. For degradation the microcarriers were immersed in PBS to evaluate their degradability and placed in a shaking incubator (80 rpm, 37 °C). At designated times, the total weight of the microcarriers was tested and compared to their initial weight. The modulus of each sample was obtained by defining the slope within the linear region. The same flattened bulk hydrogels were prepared with a gap of 1 mm. The storage modulus (G′) of the hydrogel was measured by oscillation time sweep test; the frequency was set to 1Hz, and the strain was set to 1 %.

Fibronectin coating characterization: The various microcarriers generated as described above were immersed in alcohol for half an hour and subsequently placed in a laminar flow hood for 24 h for sterilization. The microcarriers were then soaked in a fibronectin solution and shaken on a shaker for 1 h at 37 °C. To characterize whether fibronectin was coated on the microcarriers, the microcarriers were fixed with glutaraldehyde. Subsequently, immunofluorescence staining was performed on the microcarriers, with a secondary antibody labeled with FITC applied and incubated for 1 h. The microcarriers were then observed and photographed using a fluorescence microscope.

Loading of PDGF-BB: PDGF-BB was loaded onto the microcarriers using an immersion method. In brief, approximately 500 ng/mL of PDGF-BB was co-incubated with the microcarriers for 24 h in a refrigerator. For the drug release experiment, microcarriers loading PDGF-BB were incubated in a PBS solution at 37 °C in a constant-temperature shaking incubator (100 rpm), a certain amount of release solution was moved out and replaced by PBS, the release amount was detected via ELISA kit (Sigma).

Microcarrier biocompatibility and recruitment capability: Co-culture experiments were conducted by seeding Ad-MSCs (10^5 cells) and microcarriers (10 mg) on low adhesion culture plate (PVA-coated). After 24 h of incubation, the Calcein AM staining was introduced, and subsequent observation of cell growth was conducted utilizing a fluorescent microscope.

The biocompatibility test was validated using a Transwell plate. Microcarriers (5 mg) were put on the upper of Transwell plate, while Ad-MSCs (1.5×10^4 mL^{-1}) were cultured within the lower chambers in 24-well plate. CCK-8 assays were performed on cells within the lower well plate at various time points to assess their proliferative activity. On different time points the lower chambers were filled with 10 % CCK-8 solution. The OD value was measured after incubation at 37 °C for an hour.

For cell recruitment test, microcarriers (5 mg) were put on the upper of Transwell plate, and the MCF-10A cells (Wuhan Shangen Biotechnology) were cultured within the lower well plate. When the cell confluence reaches 80 %, serum-free culture medium was used to avoid the effect of proliferation. A yellow pipette tip was selected for creating

scratches across the MCF-10A cells (Wuhan Shangen Biotechnology). Cell migration was observed at 0, 12, 24 h points and the images were recorded.

In vitro photoaging: HaCaTs cells (Wuhan Shangen Biotechnology) were cultured in normal medium. While the cell confluence reached around 60 %, they were further cultured for one day using serum-free medium. The experimental group underwent ultraviolet irradiation (SH2B type UVB lamp) treatment, and the cells were covered with medium to prevent direct exposure. The control group did not undergo ultraviolet treatment. For microcarriers groups, approximately 10 mg of modified microcarriers were co-cultured with 10^5 Ad-MSCs cells for 24 h, and then the Ad-MSCs-loaded microcarrier leaching media was added into the ultraviolet treated group, the HaCaTs cells were cultured for additional 24 h. For senescence-associated β-galactosidase and γ-H2Ax immunofluorescence staining, the cultured cells were washed three times and then fixed in 4 % FPA for 15 min. The cells were then treated using freshly prepared β-galactosidase staining kits and γ-H2Ax immunofluorescence staining kits (Beyotime, Shanghai, China), respectively. The percentage of positive cells was further measured by ImageJ software.

Cellular ROS generation and apoptosis: To determine the intracellular ROS levels, different groups of photoaging model were added with suitable amount of DCFH-DA. Incubation was carried out at incubator for 20 min at 37 °C. After incubation, the cells were washed with serum-free cell culture medium and then recorded using a fluorescence microscope. For the apoptosis experiment, after fixing the cells, Apoptosis staining agents (Beyotime) were added, gently mixed, and wrapped in tinfoil at room temperature. Subsequently, the samples were then analyzed using a flow cytometer.

Animal experiment: Animal experiments were approved by University of Chinese Academy of Sciences of Wenzhou Institute (WIUCAS24010902). In photoaging model experiment, the dorsal skin of nude mice (6–8 weeks old) was exposed to UVB (Philips; emission spectrum 311 nm) positioned 15 cm above and MOP-8 (0.1 mg/ml) every other day for eight weeks. If blistering, rupture, and erosion occurred during irradiation, the exposure was stopped and the skin on the back was disinfected with povidone-iodine twice daily. This regimen continued until symptoms disappeared, after which regular irradiation resumed. For treatment, the nude mice were divided into five different groups: no UVB exposure group (Control), UVB exposure group (Model), RHC microcarrier treatment group (Group A), bare Ad-MSCs treatment group (Group B), and Ad-MSCs-loaded RHC microcarrier treatment group (Group C). The subcutaneous injection of the treatment group was administered at five different locations on the entire dorsal skin. For statistical analysis, three randomly selected areas of the dorsal skin from each group of mice were chosen. After 28 days of treatment, the nude mice were euthanized by carbon dioxide, and the dorsal skin was fixed in a polyformaldehyde solution. After paraffin embedding and sectioning, immunohistochemical staining was performed using Masson's trichrome kit from servicebio (China), and immunofluorescent staining was performed using antibodies against type I collagen, elastin elastic fibers, IL-6, TNF-a, CD31 and a-SMA from servicebio (China).

In vivo live imaging: Nude mice were divided as a MSC group and a Microcarrier group. Mice in the MSC group were treated only by Ad-MSCs and those in the Microcarrier group were injected with Ad-MSCs-loaded microcarriers. All cells were labeled with DiR. Then, a bioluminescence system (Caliper IVIS Lumina XR, America) was used for luminescence imaging. For the microcarrier degradation experiment, Ultrasoft microcarriers labeled with CY5.5 were injected subcutaneously into nude mice. The bioluminescence system was used for luminescence imaging. The signal intensity at the first time point was set as the control.

Real-time fluorescence quantitative PCR: Skin tissue around the back of the nude mice (50 mg) was collected and Trizol (1 mg) was added to acquire RNA. Further reverse transcription operations were then performed using the selected PrimeScript reverse transcription kit. The SYBR Green I fluorescent dye method was employed for PCR detection of cDNA, with primer designs detailed in Table S2.

Statistical Analysis: All paired data for comparisons were subjected to independent Student's t-tests to perform a rigorous analysis of statistical significance. Each experimental group underwent at least three repetitions to ensure robustness and reliability of the results. The criterion for significance was $p < 0.05$.

CRediT authorship contribution statement

Xiang Lin: Writing – original draft, Formal analysis, Data curation, Conceptualization. **Anne M. Filppula:** Supervision, Resources, Project administration. **Yuanjin Zhao:** Software, Resources, Project administration. **Luoran Shang:** Writing – review & editing, Supervision. **Hongbo Zhang:** Writing – review & editing, Software, Resources, Funding acquisition.

Declaration of competing interest

Yuanjin Zhao and Hongbo Zhang are editorial board members for Bioactive Materials and were not involved in the editorial review or the decision to publish this article. All authors declare that there are no competing interests.

Ethics approval and consent to participate

Animal experiments were approved by University of Chinese Academy of Sciences of Wenzhou Institute (WIUCAS24010902).

Acknowledgements

This work was supported by the National Key Research and Development Program of China (2022YFA1105300), the National Natural Science Foundation of China (52073060, 61927805 and 82400718), the Nanjing Medical Science and Technique Development Foundation (ZKX21019), the Clinical Trials from Nanjing Drum Tower Hospital (2022-LCYJ-ZD-01). This work was also supported by the Research Project (347897), Solution for Health Profile (336355), InFLAMES Flagship (337531), and "Printed Intelligence Infrastructure" (PII-FIRI)" from Research Council of Finland.

Appendix A. Supplementary data

Supplementary data to this article can be found online athttps://doi.org/10.1016/j.bioactmat.2024.12.024.

References

[1] A. Brunet, M.A. Goodell, T.A. Rando, Ageing and rejuvenation of tissue stem cells and their niches, Nat. Rev. Mol. Cell Biol. 24 (1) (2023) 45–62, https://doi.org/10.1038/s41580-022-00510-w.

[2] W.Q. Liang, Q.J. Chen, S.S. Cheng, et al., Skin chronological aging drives age-related bone loss via secretion of cystatin-A, Nature Aging 2 (10) (2022) 906, https://doi.org/10.1038/s43587-022-00285-x.

[3] T. Mauro, D. Bikle, Skin and bone crosstalk during aging, Nature Aging 2 (10) (2022) 874–875, https://doi.org/10.1038/s43587-022-00295-9.

[4] W.B. Wang, Y.D. Lin, L.M. Zhao, et al., Developmentally programmed early-age skin localization of iNKT cells supports local tissue development and homeostasis, Nat. Immunol. 24 (2) (2023) 225, https://doi.org/10.1038/s41590-022-01399-5.

[5] E. Fitsiou, T. Pulido, J. Campisi, et al., Cellular senescence and the SenescenceAssociated secretory phenotype as drivers of skin photoaging, J. Invest. Dermatol. 141 (4) (2021) 1119–1126, https://doi.org/10.1016/j.jid.2020.09.031.

[6] H.Y. Lee, E.J. Kim, D.Y. Cho, et al., Photoprotective effect of fermented and aged mountain-cultivated ginseng sprout (*Panax ginseng*) on ultraviolet radiation-induced skin aging in a hairless mouse model, Nutrients 15 (7) (2023), https://doi.org/10.3390/nu15071715, 1715. 1715.

[7] P. Pittayapruek, J. Meephansan, O. Prapapan, et al., Role of matrix metalloproteinases in photoaging and photocarcinogenesis, Int. J. Mol. Sci. 17 (6) (2016), https://doi.org/10.3390/ijms17060868, 868. 868.

[8] A. Salminen, K. Kaarniranta, A. Kauppinen, Photoaging: UV radiation-induced inflammation and immunosuppression accelerate the aging process in the skin, Inflamm. Res. 71 (7–8) (2022) 817–831, https://doi.org/10.1007/s00011-022-01598-8.

[9] M.V.P. Suyanto, I.G.A. Widianti, Protective role of melatonin in ultraviolet radiation-induced oxidative stress in human skin photoaging, Universa Medicina 42 (3) (2023) 346–359.
[10] L.G. Carter, J.A. D'Orazio, K.J. Pearson, Resveratrol and cancer: focus on *in vivo* evidence, Endocr. Relat. Cancer 21 (3) (2014) R209–R225, https://doi.org/10.1530/erc-13-0171.
[11] S.Q. Hu, Z.H. Li, J. Cores, et al., Needle-free injection of exosomes derived from human dermal fibroblast spheroids ameliorates skin photoaging, ACS Nano 13 (10) (2019) 11273–11282, https://doi.org/10.1021/acsnano.9b04384.
[12] R.R. Kotha, D.L. Luthria, Curcumin: biological, pharmaceutical, nutraceutical, and analytical aspects, Molecules 24 (16) (2019), https://doi.org/10.3390/molecules24162930, 2930. 2930.
[13] G. Lemperle, V. Morhenn, U. Charrier, Human histology and persistence of various injectable filler substances for soft tissue augmentation, Aesthetic Plast. Surg. 27 (5) (2003) 354–366, https://doi.org/10.1007/s00266-003-3022-1.
[14] J.W. Shin, S.H. Kwon, J.Y. Choi, et al., Molecular mechanisms of dermal aging and antiaging approaches, Int. J. Mol. Sci. 20 (9) (2019), https://doi.org/10.3390/ijms20092126, 2126. 2126.
[15] A. Tezel, G.H. Fredrickson, The science of hyaluronic acid dermal fillers, J. Cosmet. Laser Ther. 10 (1) (2008) 35–42, https://doi.org/10.1080/14764170701774901.
[16] F. Wang, L.A. Garza, S. Kang, et al., In vivo stimulation of de novo collagen production caused by cross-linked hyaluronic acid dermal filler injections in photodamaged human skin, Arch. Dermatol. 143 (2) (2007) 155–163, https://doi.org/10.1001/archderm.143.2.155.
[17] S.H. Li, Y.H. Liu, T. Zhang, et al., A tetrahedral framework DNA-based bioswitchable miRNA inhibitor delivery system: application to skin anti-aging, Adv. Mater. 34 (46) (2022) 2204287, https://doi.org/10.1002/adma.202204287.
[18] A.H. Qu, Q.W. Chen, M.Z. Sun, et al., Sensitive and selective dual-mode responses to reactive oxygen Species by chiral manganese dioxide nanoparticles for antiaging skin, Adv. Mater. 36 (5) (2024) 202308469, https://doi.org/10.1002/adma.202308469.
[19] J. Campisi, Senescent cells, tumor suppression, and organismal aging: good citizens, bad neighbors, Cell 120 (4) (2005) 513–522, https://doi.org/10.1016/j.cell.2005.02.003.
[20] S.H. He, N.E. Sharpless, Senescence in health and disease, Cell 169 (6) (2017) 1000–1011, https://doi.org/10.1016/j.cell.2017.05.015.
[21] C. López-Otín, M.A. Blasco, L. Partridge, et al., The hallmarks of aging, Cell 153 (6) (2013) 1194–1217, https://doi.org/10.1016/j.cell.2013.05.039.
[22] S.J. Morrison, A.C. Spradling, Stem cells and niches: mechanisms that promote stem cell maintenance throughout life, Cell 132 (4) (2008) 598–611, https://doi.org/10.1016/j.cell.2008.01.038.
[23] R.J. Brentjens, M.L. Davila, I. Riviere, et al., CD19-Targeted T cells rapidly induce molecular remissions in adults with chemotherapy-refractory acute lymphoblastic leukemia, Sci. Transl. Med. 5 (177) (2013) 177ra38, https://doi.org/10.1126/scitranslmed.3005930.
[24] J. Chen, Y.J. Li, T.S. Yu, et al., A restricted cell population propagates glioblastoma growth after chemotherapy, Nature 488 (7412) (2012) 522, https://doi.org/10.1038/nature11287.
[25] M. Nie, G.P. Chen, C. Zhao, et al., Bio-inspired adhesive porous particles with human MSCs encapsulation for systemic lupus erythematosus treatment, Bioact. Mater. 6 (1) (2021) 84–90, https://doi.org/10.1016/j.bioactmat.2020.07.018.
[26] M. Nie, B. Kong, G.P. Chen, et al., MSCs-laden injectable self-healing hydrogel for systemic sclerosis treatment, Bioact. Mater. 17 (2022) 369–378, https://doi.org/10.1016/j.bioactmat.2022.01.006.
[27] Z.H. Chen, Z.D. Lv, Y.P. Zhuang, et al., Mechanical signal-tailored hydrogel microspheres recruit and train stem cells for precise differentiation, Adv. Mater. 35 (40) (2023) 202300180, https://doi.org/10.1002/adma.202300180.
[28] B.F. Wang, Y.W. Li, M.F. Zhou, et al., Smartphone-based platforms implementing microfluidic detection with image-based artificial intelligence, Nat. Commun. 14 (1) (2023), https://doi.org/10.1038/s41467-023-36017-x, 1341. 1341.
[29] Y.C. Wang, H. Jeon, 3D cell cultures toward quantitative high-throughput drug screening, Trends Pharmacol. Sci. 43 (7) (2022) 569–581, https://doi.org/10.1016/j.tips.2022.03.014569.
[30] Y.H. Wang, G.X. Zheng, N. Jiang, et al., Nature-inspired micropatterns, Nature Reviews Methods Primers 3 (1) (2023), https://doi.org/10.1038/s43586-023-00251-w, 68. 68.
[31] N. Yang, W. Song, Y. Xiao, et al., Minimum minutes machine-learning microfluidic microbe monitoring method (M7), ACS Nano 18 (6) (2024) 4862–4870, https://doi.org/10.1021/acsnano.3c09733.
[32] J. He, Y. Sun, Q. Gao, et al., Gelatin methacryloyl hydrogel, from standardization, performance, to biomedical application, Adv. Healthcare Mater. 12 (23) (2023) 202300395, https://doi.org/10.1002/adhm.202300395.
[33] B. Kong, R. Liu, X.J. Hu, et al., Cornea-Inspired ultrasound-responsive adhesive hydrogel patches for keratitis treatment, Adv. Funct. Mater. 34 (12) (2024) 202310544, https://doi.org/10.1002/adfm.202310544.
[34] C.G. Ouyang, H.J. Yu, L. Wang, et al., Tough adhesion enhancing strategies for injectable hydrogel adhesives in biomedical applications, Adv. Colloid Interface Sci. 319 (2023) 102982, https://doi.org/10.1016/j.cis.2023.102982.
[35] Y. Zhu, B. Kong, R. Liu, Y. Zhao, Developing biomedical engineering technologies for reproductive medicine, Smart Medicine 1 (1) (2022) e20220006.
[36] O. Chaudhuri, L. Gu, D. Klumpers, et al., Hydrogels with tunable stress relaxation regulate stem cell fate and activity, Nat. Mater. 15 (3) (2016) 326, https://doi.org/10.1038/nmat4489.
[37] C. López-Otín, M.A. Blasco, L. Partridge, et al., Hallmarks of aging: an expanding universe, Cell 186 (2) (2023) 243–278.
[38] K.-K. Tian, S.-C. Huang, X.-X. Xia, Z.-G. Qian, Fibrous structure and stiffness of designer protein hydrogels synergize to regulate endothelial differentiation of bone marrow mesenchymal stem cells, Biomacromolecules 23 (4) (2022) 1777–1788.